Development of pore water pressure around a stone column.

Développement des pressions interstitielles autour d'une colonne ballastée.

Gautray J., Laue J., Springman S.M.
Institute for Geotechnical Engineering, ETH Zürich, Switzerland

Almeida M.
Federal University of Rio de Janeiro, Rio de Janeiro, Brazil

ABSTRACT: The bearing capacity of model stone columns installed in soft soil is investigated in a series of centrifuge model tests that are carefully instrumented to reveal the response of the ground during penetration of the tool and the cyclic compaction process during withdrawal. Pore pressures are measured at various distances from the column axes as well as at different depths, and the influence of the excess pore water pressure build up and dissipation around the column and the development of the load transfer mechanism are examined. The data are analysed and compared to theoretical solutions, both for the installation phase of the column as well as for subsequent loading with a stiff, circular foundation. These provide a set of high quality data for validating numerical methods. The measurements, and the associated analyses, will help to determine the transient load bearing capacity of stone columns and the effects of accelerated pore pressure dissipation, which will contribute to improving the understanding and use of this mode of ground improvement.

RÉSUMÉ : Une recherche sur la capacité portante de modèles de colonnes ballastées installées dans un sol mou est réalisée dans une série d'essais en centrifugeuse instrumentés avec soin afin de mettre en exergue la réponse du sol durant la pénétration de l'outil ainsi que le processus de compaction cyclique durant l'extraction. Les pressions interstitielles sont mesurées à différentes distances de l'axe de la colonne ainsi qu'à différentes profondeurs et l'influence de la formation et de la dissipation des surpressions interstitielles autour de la colonne et le développement du mécanisme de transfert de charge sont examinés. Les données sont analysées et comparées avec des solutions théoriques pour la phase d'installation de la colonne et pour le chargement consécutif avec une fondation circulaire rigide, fournissant une série de données de haute qualité pour la validation de méthodes numériques. Les mesures, ainsi que les analyses associées, aideront à déterminer la capacité portante de colonnes ballastées ainsi que les effets de la dissipation accélérée des pressions interstitielles, ce qui contribuera à améliorer la compréhension et l'utilisation de ce mode d'amélioration des sols.

KEYWORDS: Ground improvement, stone columns, consolidation

1 INTRODUCTION

Stone columns have proven to be an efficient ground improvement technique. They increase the vertical stiffness and reduce the consolidation time, as radial drainage dominates the consolidation process (e.g. Hansbo, 1981).

This paper presents the results of a centrifuge test conducted in the ETH Zürich geotechnical drum centrifuge (Springman et al., 2001) at multiple earth's gravity, n = 50. A stone column has been installed in a clay model (Weber, 2008) and is loaded with a circular footing. The pore pressures developing during installation and the loading phase were recorded and studied.

2 SOILS

2.1 *Soft clay bed - Birmensdorf clay*

Remoulded natural clay from the traffic interchange near to Birmensdorf was consolidated in a large oedometer and used as soft clay bed for the experiment. The main properties of this clay are summarised in Table 1.

2.2 *Granular column – quartz sand*

As tested by Weber (2008), quartz sand (fraction 0.5 – 1 mm) was used for constructing the sand columns (see Table 2).

Table 1: Properties of the reconstituted Birmensdorf clay (after Weber, 2008).

USCS classification	CH
Clay particle content from sedimentation analysis < 2μm [%]	42
Liquid limit w_l [%]	45-62 (av. 60)
Plastic limit w_p [%]	18-26 (av. 21)
Plasticity index I_p [%]	27-36 (av. 30)
Critical state angle of friction ϕ'_{cv} [°]	24.5
Cohesion c' [kN/m^2]	0
Specific density ρ_s [g/cm^3]	2.75
Medium grain size d_{50} [μm]	4
Water-saturated permeability k [m/s] for a void ratio of e = 1.10 [-]	$1.5.10^{-9}$

2.3 *Filling material - Perth sand*

Perth sand was used in order to fill the gap between the clay model and the wall of the model container (see Fig. 1). Selected properties of this material can also be found in Table 2.

Table 2: Selected sand properties i) column (Weber, 2008) ii) Perth sand (Buchheister, 2009).

Origin	Column	Perth
USCS classification	SP	SP
Density ρ_s [g/cm^3]	2.65	2.65
Critical state angle of friction ϕ'_{cv} [°]	37.0	30.5
Medium grain size d_{50} [mm]	0.75	0.23
Coefficient of uniformity [-]	1.4	1.79
Coefficient of gradation [-]	1.0	1.26
Grain shape	semi-angular-slightly rounded	-

3 SAMPLE PREPARATION

The clay was consolidated in a 250 mm diameter oedometer with incremental loading up to a total vertical stress of 200 kPa. The sample was removed from the oedometer container and the pore pressure transducers (PPTs) were installed. Their locations are shown in Fig. 1. The sample was then put into the centrifuge strongbox (diameter 400 mm) and the gap of 75 mm between container wall and clay model was filled with Perth sand by dry pluviation without compaction (Fig. 1), resulting in an axisymmetric sample. In this test, the boundary conditions cannot be considered to be oedometric with no radial strain, as the sand/clay interface is not rigid.
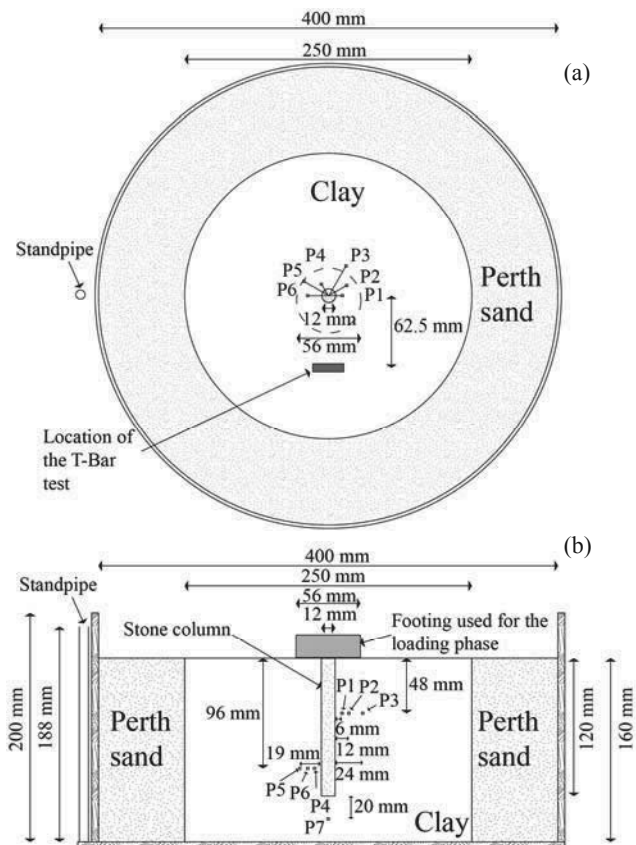

Fig. 1: (a) Plan view and (b) cross-section of the model set-up.

4 T-BAR TEST

A T-bar test, the location of which can be seen in Fig. 1, was conducted in order to determine the profile of the undrained shear strength in the soft clay. The T-bar (Fig. 2) has a length of 28 mm and a diameter of 7 mm. It was driven at a rate of 0.5 mm/s up to a depth of 140 mm, where a waiting time of one

minute was observed before the tool was pulled back out of the model.

The undrained shear strength was calculated with the following equation:

$$s_u = \frac{F}{L \cdot B \cdot N_b} \ [kPa] \qquad (5)$$

where F is the force recorded for the T-bar penetration, L the length of the T-bar, B the width of the T-bar and N_b the T-bar factor, set in this case at 10.5 [-] (Stewart et al., 1994).
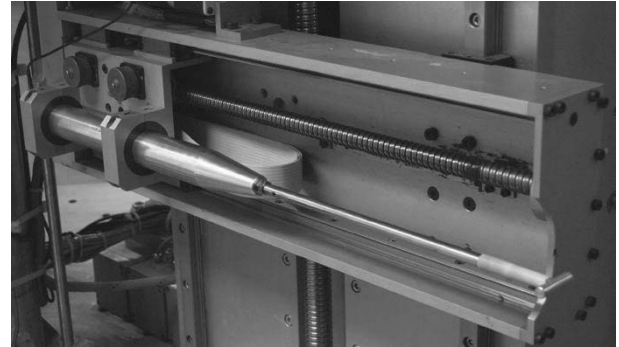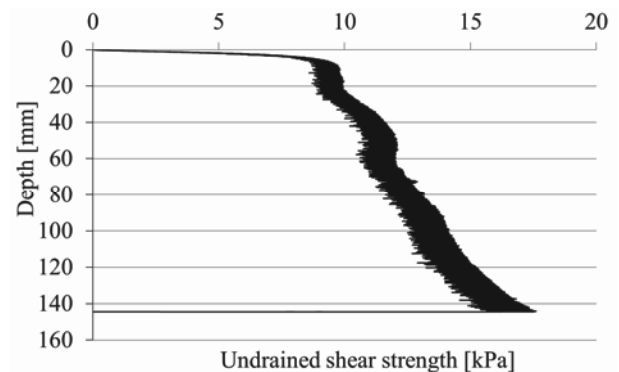

Fig. 2: T-bar (Weber, 2008).

Fig. 3: Profile of the undrained shear strength obtained with the T-Bar.

5 INSTALLATION OF THE STONE COLUMN

The test procedure and the corresponding results are presented at model scale with the exception of the forces, which are scaled to prototype scale. According to the scaling relationships, stresses are scaled by the factor 1, whereas time scaling from model to prototype differs by a factor n^2 for diffusion processes and by n during inertia processes. Forces are scaled by a factor n^2 (e.g. Schofield, 1980), n being the factor by which earth's gravity is increased.
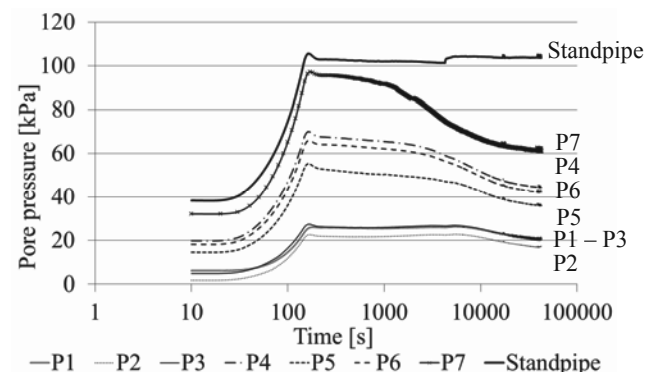

Fig. 4: Evolution of the pore water pressures during the in-flight consolidation.

5.1 *Consolidation*

The first step in the centrifuge model test is to reconsolidate the clay model in-flight at an acceleration of 50 g, due to the increase in self-weight. Dissipation of the excess pore water pressures took approximately 13 h (Fig. 4).

5.2 *Stone column installation*

The stone column installation tool developed by Weber (Fig. 5; Weber, 2008) has been used to construct the stone column. It consists of a steel tube with an outer diameter of 10 mm and an inner diameter of 8 mm. A drawing pin was used to prevent the tube from blocking during first penetration.
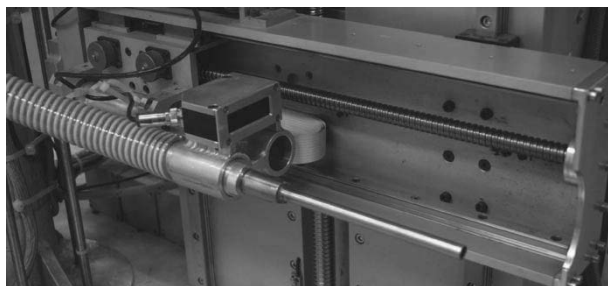

Fig. 5: Stone column installation tool (Weber, 2008).

The column tool was inserted up to a depth of 120 mm in the centre of the clay model and the column was built with a 15/10 compaction regime (i.e. once the desired installation depth was reached, the tool was extracted by 15 mm before being inserted again 10 mm, compacting the sand in the column). This compaction process increases the stone column diameter to 12 mm (see Fig. 1), at least in the softest clay layer near the surface. The insertion was displacement-controlled (2 mm/s) and the driving force as well as the pore water pressures were recorded during this phase (Fig. 6). The development of pore water pressure over time is given in the top part of Fig. 6. The middle part of Fig. 6 shows the scaled driving force required to penetrate the installation tool and the bottom part shows the position of the tip of the installation tool under the surface. It can be seen that the strongest reaction of the PPTs is observed when the tip of the column tool reaches the depth of the sensors (marked by horizontal dashed lines in the Fig. 6c). This is observed both for the penetration phase and the compaction phase, respectively.

90% of the excess pore water pressures are dissipated after about 2300 s, which, when scaled by 50^2, corresponds to a prototype time of about 67 days. This is significantly shorter than the time needed for dissipation of excess pore pressures at the beginning of the test (see Fig. 4). Indeed, for a drainage path of 4 m (half of the prototype height of the model) and a one dimensional stiffness modulus $M_E = 1780$ kPa, a coefficient of consolidation $c_v = 2.67 \cdot 10^{-7} \ m^2/s$ is obtained, leading to a consolidation time at 90% excess pore water pressure dissipation of $t_{90} = T_{v90} \cdot d^2 / c_v \approx 589 \ days$. This reduces the time by a factor of 8.8, which is consistent with a combined drainage condition, i.e., vertical plus radially outwards (to the surrounding Perth sand) and inwards (towards the stone column) resulting from the insertion of the granular column.

6 FOOTING LOADING

As the third step in the test, the newly built stone column was loaded with a 56 mm-diameter stiff aluminium footing, after the excess pore water pressures caused by the installation of the column had dissipated. The loading was displacement-controlled (v = 0.02 mm/s) and a maximum settlement of 17 mm at model scale was attained before the footing was

removed and the loading-induced excess pore water pressures were left to dissipate. The first jump in excess pore water pressures (Fig. 7 top) between 0 and 1000 s is due to a technical problem, which triggered an unexpected loading of the stone column. The actual loading can thus be studied after 1000 s.

The sensors P1 (top layer close to the column) and the sensors P4, P5 and P6 in a depth of 96 mm below ground surface react in parallel to the loading, albeit with different magnitudes of pore pressure change, while P2 and P3 exhibit a less sharp response. This confirms that the column takes a larger part of the load than the soft clay and the pressure distribution with depth is not building up as it would in a homogeneous medium. Secondly, an explanation was sought for the increase (P1 to P6) or drop (P7) in pore water pressures that can be seen at about 1500 s, which might have coincided with failure of the column. A bulge could be identified in the upper third of the column as the model was being dismantled. The cause might be attributed to the development of this 'local compression failure zone' in the sand column.
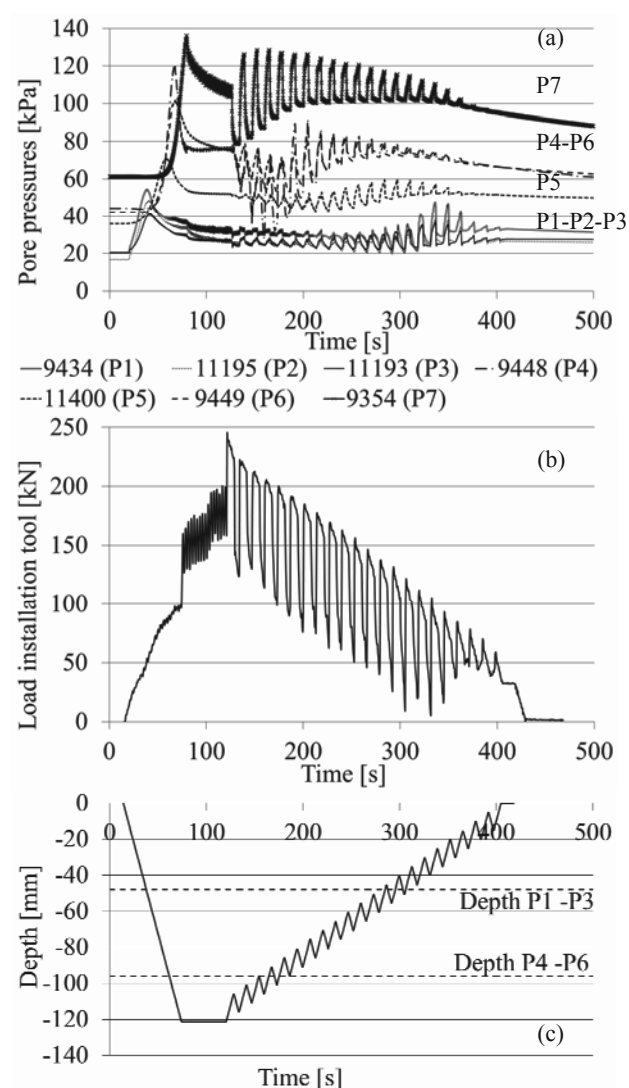

Fig. 6: (a) Pore water pressures, (b) driving force (c) depth of the tip of the installation tool during the sand column installation.

The total load applied on the footing can be formulated as (Adam, 2011):

$$\sigma_v = \left(\sigma_{sc} \cdot A_{sc} + \sigma_{clay} \cdot A_{clay} \right) / \left(A_{sc} + A_{clay} \right) \qquad (1)$$

with the corresponding load on the stone column as (Adam, 2011):

$$\sigma_{sc} = \left(1 - \sin \varphi'_{sc} \right) \cdot \left(\sigma_{clay} + 2 \cdot c_{clay} \right) / \left(1 - \sin \varphi'_{sc} \right) \qquad (2)$$

where A corresponds to the area and the indices "v" and "sc" to vertical and stone column, respectively. The load on the stone column when the jump was observed, for a global loading of 65 kPa, is then derived to be $\sigma_{sc} = 234.2\ kPa$.

Bergado et al. (1994) suggest the bulging failure load (Muir Wood et al., 2000) on a stone column is calculated from:

$$q_{max} = \left(\gamma_c \cdot z \cdot K_{p,c} + 2 \cdot s_u \cdot \sqrt{K_{p,c}} + q_0 \cdot K_{p,c}\right)\cdot\left(1+\sin\varphi_s'\right)/\left(1-\sin\varphi_s'\right) \quad (3)$$

where γ_c is the unit weight of clay, z is the depth, $K_{p,c}$ is the clay coefficient of passive earth failure, s_u is the undrained shear strength, q_0 is the overburden pressure and $\Box'_s$ is the angle of friction of the column material. A failure load of $q_{max} = 269.6\ kPa$ can be obtained.

Hughes & Withers (1974) propose a different equation to calculate the bulging failure load:

$$q_{max} = \left(\gamma_c \cdot z + 4 \cdot s_u\right)\cdot\left(1+\sin\varphi_s'\right)/\left(1-\sin\varphi_s'\right) \quad (4)$$

where the nomenclature used is the same as in the formula of Bergado et al. (1994). In this case, a failure load of $q_{max} = 209.8\ kPa$ is obtained.
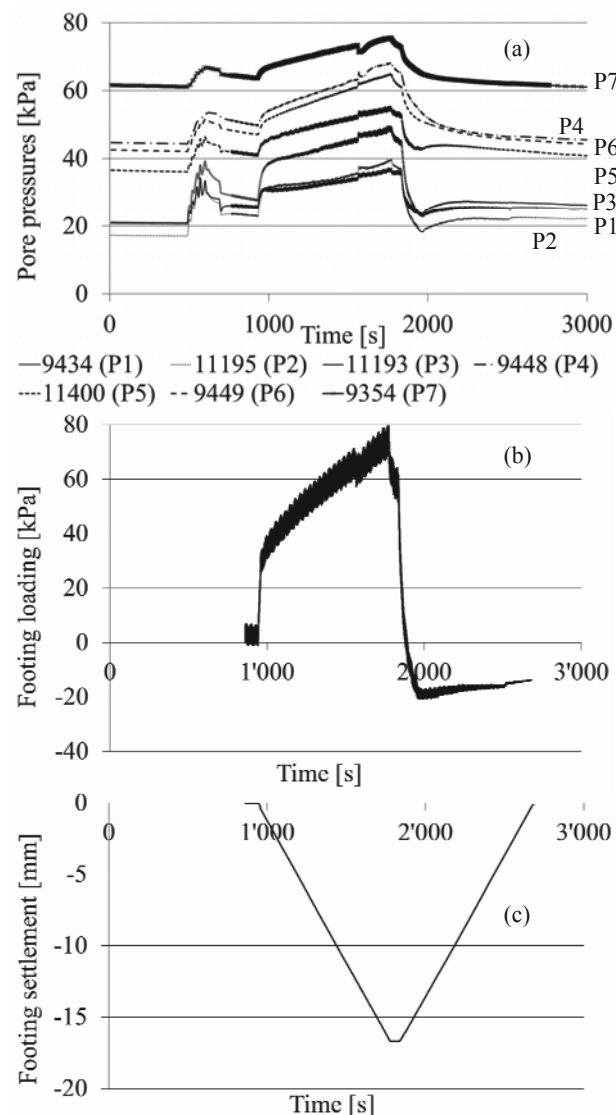

Fig. 7: (a) Pore water pressures, (b) footing loading and (c) footing settlement during the footing loading.

It can be seen that the two theoretical solutions proposed bound the value calculated from the data. As a consequence, it may be concluded that local bulging failure in the stone columns triggered an additional radial loading of the soft clay and caused a small load decrement below the column (marked

by the pore water pressure drop observed at P7, which subsequently consolidated out exponentially).

The local bulging failure described by Muir Wood et al. (2000) replicates the case of an axially loaded cylindrical specimen in a triaxial apparatus, in which shear discontinuities are formed as sections of the cylindrical specimen spall outwards from the central axis (Desrues et al., 1996).

7 SUMMARY

Data from a physical model test in a geotechnical centrifuge is provided in this contribution to validate numerical processes to simulate the installation effects of stone columns and their subsequent use as ground improvement under a footing. Pore pressure transducers have been installed in the vicinity and under the stone column in this axisymmetric test. This measurement provides valuable insight in the behaviour of the stone columns. These measurements enable the identification of the bulging failure load of the column, which lay between boundaries given by two analytical solutions.

8 ACKNOWLEDGEMENTS

9 REFERENCES

Adam. D. 2011. Bodenverbesserung versus Hybridgründung und Tieffundierung – Vergleich der Gründungskonzepte von drei Projekten mit Tragweite für Europa. *Institut für Geotechnik, ETH Zürich, Kolloquium, 17.11.2011,* www.igt.ethz.ch.

Bergado, D.T., Chai, J.C., Alfaro, M.C. and Balasubramaniam, A.S. 1994. *Improvement Techniques of Soft Ground in Subsiding and Lowland Environment.* Balkema, Rotterdam.

Buchheister, J. 2009. *Verflüssigungspotential von reinem und siltigem Sand unter multiaxialer Belastung.* Institut für Geotechnik, ETH Zürich, Diss. Nr. 18312, VDF-Verlag, ETH Zürich

Desrues, J., Chambon, R., Mokni, M. and Mazerolle, F. 1996. Void ratio evolution inside shear bands in triaxial sand specimens studied by computed tomography. *Géotechnique* 46 (3), 529-546.

Hansbo, S. 1981. Consolidation of fine-grained soils by prefabricated drains. *X ICSMFE, Stockholm, Sweden* (3), 677-682.

Hughes, J.M.O. and Withers, N.J. 1974. Reinforcing of soft cohesive soils with stone columns. *Ground Engineering* 7 (3), 42-49.

Muir Wood, D., Hu, W. and Nash, D.F.T. 2000. Group effects in stone column foundations model tests. *Géotechnique* 50 (6), 689-698.

Schofield, A.N. 1980. Cambridge geotechnical centrifuge operations: 20th Rankine lecture. *Géotechnique.* 30 (2), 129-170.

Springman, S., Laue, J., Boyle, R., White, J. and Zweidler, A. 2001. The ETH Zurich Geotechnical Drum Centrifuge. *International Journal of Physical Modelling in Geotechnics* 1 (1), 59-70.

Stewart, D.P. and Randolph, M.F. 1991. A new site investigation tool for the centrifuge. *Centrifuge '91, H.Y. Ko and F.G. McLean (eds). Balkema*, 531-537.

Weber, T.M. 2008. *Modellierung der Baugrundverbesserung mit Schottersäulen.* Institut für Geotechnik, ETH Zürich, Diss. Nr. 17321, VDF-Verlag, ETH Zürich.